Available online at www.sciencedirect.com
SCIENCE DIRECT®
Fusion Engineering and Design 72 (2005) 363–375
Fusion Engineering and Design
www.elsevier.com/locate/fusengdes

Erosion, transport, and tritium codeposition analysis of a beryllium wall tokamak☆

Jeffrey N. Brooks[a,*], Jean Paul Allain[a], Darren A. Alman[b], David N. Ruzic[b]

[a] *Argonne National Laboratory, 9700 South Cass Avenue, Argonne, IL 60439, USA*
[b] *University of Illinois, 103 South Goodwin Avenue, Urbana, IL 61801, USA*

Received 7 January 2004; received in revised form 21 September 2004; accepted 7 October 2004
Available online 9 December 2004

Abstract

We analyzed beryllium first wall sputtering erosion, sputtered material transport, and T/Be codeposition for a typical next-generation tokamak design—the fusion ignition research experiment (FIRE). The results should be broadly applicable to any future tokamak with a beryllium first wall. Starting with a fluid code scrapeoff layer attached plasma solution, plasma D^0 neutral fluxes to the wall and divertor are obtained from the DEGAS2 neutral transport code. The D^+ ion flux to the wall is computed using both a diffusive term and a simple convective transport model. Sputtering coefficients for the beryllium wall are given by the VFTRIM-3D binary-collision code. Transport of beryllium to the divertor, plasma, and back to the wall is calculated with the WBC+ code, which tracks sputtered atom ionization and subsequent ion transport along the SOL magnetic field lines. Then, using results from a study of Be/W mixing/sputtering on the divertor, and using REDEP/WBC impurity transport code results, we estimate the divertor surface response. Finally, we compute tritium codeposition rates in Be growth regions on the wall and divertor for D–T plasma shots using surface temperature dependent D–T/Be rates and with different assumed oxygen contents. Key results are: (1) peak wall net erosion rates vary from about 0.3 nm s^{-1} for diffusion-only transport to 3 nm s^{-1} for diffusion plus convection, (2) T/Be codeposition rates vary from about 0.1 to 10.0 mg T s^{-1} depending on the model, and (3) core plasma contamination from wall-sputtered beryllium is low in all cases (< 0.02%). Thus, based on the erosion and codeposition results, the performance of a beryllium first wall is very dependent on the plasma response, and varies from acceptable to unacceptable.

Keywords: Tritium codeposition; Beryllium; Tokamak

1. Introduction

The sputtering performance of plasma-facing components (PFCs) surface materials is critical to future fusion devices. The critical issues are: (1) net erosion rates and lifetime, (2) tritium codeposition in redeposited

☆ Work supported by the U.S. Department of Energy, Office of Fusion Energy.
* Corresponding author. Tel.: +1 630 252 4830; fax: +1 630 252 3250.
E-mail address: brooks@anl.gov (J.N. Brooks).

0920-3796/$ – see front matter © 2004 Elsevier B.V. All rights reserved.
doi:10.1016/j.fusengdes.2004.10.002

materials, and (3) core plasma contamination. As recently reviewed in [1], erosion/redeposition codes have been extensively used to assess PFC sputtering performance, with most of the focus, however, being on single-material divertor or limiter surfaces. There has been much less work done on wall erosion, and on mixed material surfaces.

We take as a test-bed for this study, the fusion ignition research experiment (FIRE) design [2]. FIRE is a tokamak design with the goal of exploring the next frontier in magnetic fusion, that being the study of the physics in a self-heated fusion plasma, in a device with the minimum necessary size and low relative cost. FIRE is a compact, high current, high magnetic field machine with major radius 2.14 m, 10 T field, 20 s flat top time, and 150 MW of fusion power. The duty factor is of order 1%. The design calls for a beryllium first wall with a thickness of 5 mm to be plasma-sprayed onto copper tiles. The divertor design is tungsten rods on a CuCrZr heat sink.

FIRE may or may not be built. However, the analysis here should apply generally to any next-generation tokamak, in particular ITER, although specific quantitative estimates would need revision based on exact geometry, plasma conditions, etc.

A beryllium wall coating offers low Z plasma contamination and the added advantages of good oxygen gettering and the ability to re-coat the walls in situ. Because of high erosion rates other wall materials will eventually be needed for high duty-factor fusion devices such as a DEMO reactor. General considerations for sputtering erosion of beryllium plasma facing components and specific analysis for the ITER design beryllium wall with a detached plasma regime were discussed in [3]. That work concluded that although a beryllium wall performs better than a carbon wall, there is still concern about erosion rates and significant concern about tritium codeposition. The codeposition issue is of particular concern to FIRE because the in-vessel tritium limit is low, of order 10 g. Study [3] also pointed out the need for more detailed calculations of wall-sputtered material transport. Such calculations have now been done in the present work.

Tungsten is a good divertor material for any device, from the sputtering erosion standpoint, being a high surface temperature material with very low erosion for edge plasma temperatures $\leq$50 eV. Previous work showed essentially zero net erosion of a pure tungsten divertor plate in FIRE [4], with no plasma contamination, for an attached plasma with conditions $T_e = 15$ eV, $n_e = 2 \times 10^{21}$ m^{-3} at the strike point. This is due to the short ionization mean-free path for sputtered tungsten atoms ($\sim$25 μm) and high sheath acceleration and collisional induced flow of tungsten ions back to the divertor. Tritium codeposition in tungsten is likewise insignificant due to low/zero erosion to begin with and low hydrogen isotope Q/W trapping rates. A concern, however, is the effect of Be/W mixing on the divertor and resulting mixed-material performance, including disruption/ELM response. Thus, another goal of this study is to compute wall-sputtered beryllium flux to the divertor for use in analysis of the mixing issue.

In general, the present study for the FIRE design is important to understand generic plasma/surface interaction issues in any near-term fusion tokamak.

2. Computational method

Wall erosion and transport analysis is complicated. First, the plasma parameters (density, temperature, flow velocities, etc.) for the FIRE tokamak edge must be specified. Second, calculations are needed for the wall neutral atom flux arising from ion recycling at the walls and divertor, and by fueling. Then to be computed is sputtering of the wall beryllium coating by impinging ions and neutrals. Then, the transport of wall-sputtered beryllium through the scrape off layer plasma to the core plasma, divertor, and back to the wall must be calculated. Then, erosion/redeposition of the mixed Be/W divertor must be assessed. Finally, plasma contamination potential and codeposition rates can be estimated.

No one single computer code exists to solve all of the sub-problems listed above. Therefore, this work required a coupling of six different computer codes in the steps outlined below. Ideally, these codes should be self-consistently coupled, such coupling done in real-time. This is not the case presently and remains a future goal for all fusion programs. We discuss later some issues of code consistency.

2.1. Solution for plasma parameters with the UEDGE fluid code

UEDGE is a time dependent, 2-D fluid code that models the edge plasma region of a tokamak [5]. An

MHD equilibrium, which gives the magnetic flux surfaces, provides the basis for the UEDGE simulation geometry. Boundary conditions of the densities and temperatures in the core region, and particle recycling coefficients at walls and divertor plates, are specified as inputs to the code. By solving the equations for particle continuity, parallel momentum, electron and ion energy, electrostatic potential, and neutral gas diffusion, UEDGE provides plasma ion and electron densities, temperatures, flow velocities, and currents to the divertor plates.

The FIRE case analyzed [6] is attached plasma with 175 A of neon injection resulting in peak ion densities of $5.2 \times 10^{21}\,\mathrm{m}^{-3}$ and $1.5 \times 10^{22}\,\mathrm{m}^{-3}$, and electron temperatures of 15 and 1.5 eV at the outer and inner divertor plates, respectively. The dominant neutral source is the ion current to the outboard divertor plate of $1.1 \times 10^{24}\,\mathrm{s}^{-1}$.

A note: the FIRE cases of most interest are D–T plasmas. Following the UEDGE calculation scheme, however, we are not treating tritium explicitly in our neutral, and sputtering calculations, but instead are using deuterium parameters to apply to a D–T mixture. For the purposes of this paper any isotopic effects, e.g. mass differences in sputter yields, are minor compared with uncertainties such as convection transport terms. In estimating tritium codeposition, however, we explicitly assume an equal part D–T plasma.

2.2. Extending the UEDGE plasma solution to the real wall location

The UEDGE solution in its original form gives the flux of ions only to the divertor plates, and not to the first wall. In particular, the UEDGE geometry ends about 3 cm short of the wall location. (This is reasonable because the ion flux to the wall is critical to the erosion problem studied here, but not to obtaining the basic UEDGE SOL plasma). Here, we are interested in the flux to the wall to calculate beryllium erosion. To calculate an ion flux to the wall, as well as to track neutrals and later beryllium impurities through the near-wall plasma, the UEDGE plasma solution was extended outward to the real wall location.

To do this, we developed a code, U-READER, that is capable of loading a UEDGE data file, visualizing the geometry and data (e.g. able to view and identify coordinates on the computational mesh or create contour plots of temperature and density), modifying the geometry by adding new zones beyond the original UEDGE boundary, extrapolating the plasma parameters into the new zones, calculating ion fluxes to the new boundaries (i.e. first wall), and finally saving the new plasma data in a format easily incorporated into the DEGAS2 code, which is used in the next step of this procedure. The U-READER code could be extended to further interface with DEGAS2, for example by graphically setting up the polygons that define the DEGAS2 geometry.

The code opens the original UEDGE data file and a second input file that contains the specification of the wall location. The desired number of new radial zones is specified in the graphical interface and the new grid points for the extended mesh are extrapolated linearly from the outermost points in the UEDGE geometry, until they reach the wall. Plasma parameters for each new, empty zone are extrapolated from the outermost UEDGE zones according to their radial coordinate. For example, the ion density outward a distance x from the last zone is given by:

$$n_i(x) = n_0 \exp\left(\frac{-x}{\lambda}\right) \tag{1}$$

where n_0 is the density at the last UEDGE zone and λ the scrape-off length fit to the pre-existing UEDGE zones.

The ion flux to the first wall is calculated as the sum of a cross-field diffusion term, an anomalous transport term, and (possibly) a convective transport term giving:

$$\Gamma_\perp = -D_\perp \nabla n_i - D_{\mathrm{anomalous}} \nabla n_i + n_i V_{\mathrm{conv}} \tag{2}$$

The issue of a convective term has been noted for many years. Higher fluxes of ions and neutrals appear to exist in the edge of a tokamak [7] than accounted for by cross-field diffusion [8], unless one uses a radially varying diffusion coefficient which increases dramatically at the wall [9]. The convective transport may be due to large-scale structures of plasma with high radial velocity [10], and is likely related to the "blob" or "avaloid" transport noted recently in several machines. Here, more standard diffusion coefficients are maintained, but a convective term is specifically added.

The perpendicular diffusion coefficient is assumed to be $0.1\,\mathrm{m}^2\,\mathrm{s}^{-1}$, the anomalous diffusion coefficient is $0.1\,\mathrm{m}^2\,\mathrm{s}^{-1}$ as in UEDGE [6], and the convective velocity is assumed to be $100\,\mathrm{m}\,\mathrm{s}^{-1}$ at the wall, correspond-

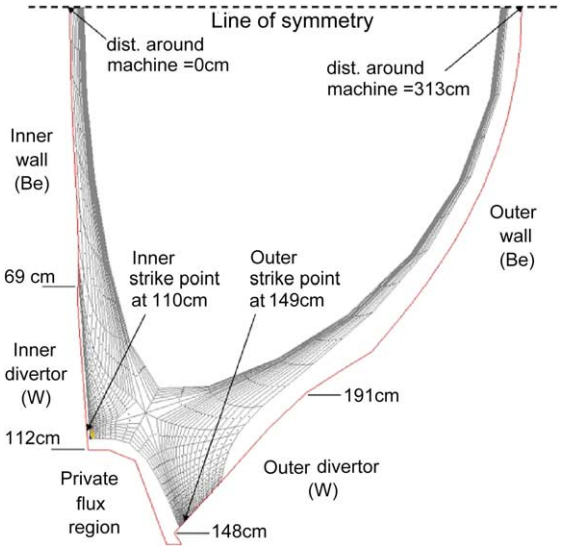

Fig. 1. Original computational domain from UEDGE, shown with the real wall location. The ∼3 cm of empty space was filled in with the extrapolated plasma parameters. Quoted wall locations are measured from the inner midplane, counter-clockwise around the machine to the outer midplane.

ing to recent estimates [6,11]. Convective transport was found to dominate the flux calculation. Therefore, two cases were run, one with and one without convective transport.

The initial geometry obtained from UEDGE is shown in Fig. 1. The real wall location is also shown, illustrating the 3 cm space that had to be filled in. After the mesh was extended, density and temperature profiles can be obtained for the entire lower half of the symmetric double null machine, as in Fig. 2.

2.3. DEGAS2 neutral transport modeling

DEGAS2 [12] is a Monte Carlo code for studying neutral atom and molecular transport in fusion plasmas. It is an improved version of DEGAS [13], with the advantages of increased flexibility due to its quasi-object oriented design and improved coding standards, easier use and better documentation, better performance, and more portability across different platforms. It takes the modified UEDGE geometry and background plasma specification discussed above as input.

Neutrals are created from ion recycling at the walls (given by the model above) and divertor plates (given

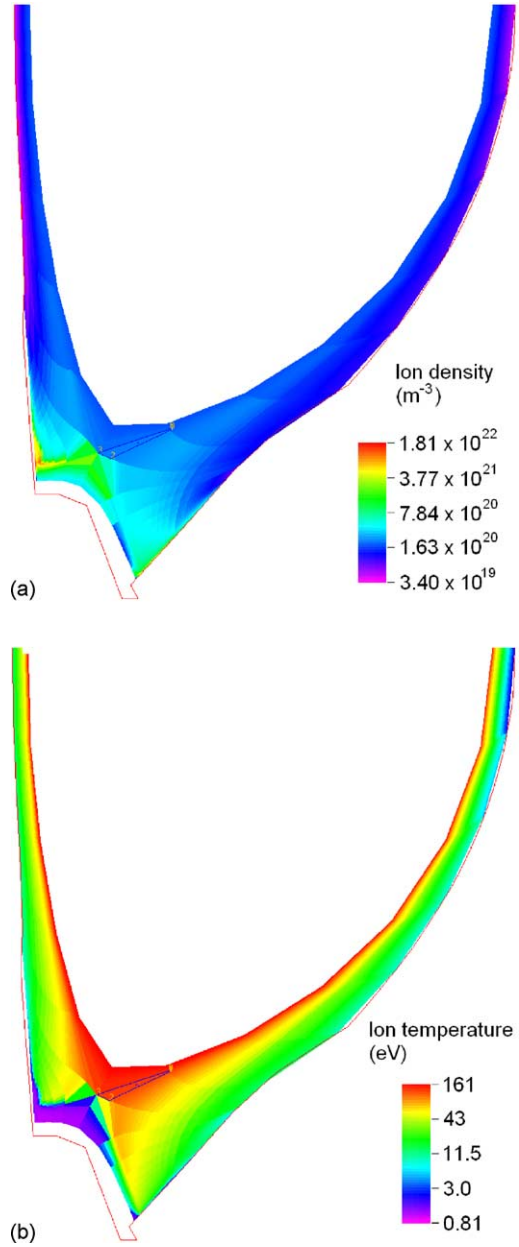

Fig. 2. The extended plasma, showing the (a) density and (b) temperature contours.

by UEDGE), recombination, and fueling). Fueling is added to be within FIRE's design parameters of a total fueling rate of 200 Torr-l s^{-1}, with 100–175 Torr-l s^{-1} to come from gas puffing and 25–100 Torr-l s^{-1} to come from pellet injection. In this work we have as-

sumed 100 Torr-l s^{-1} of both gas puffing and pellet injection. The pellet injection is added as a neutral source from the core boundary. Gas puffing was added to the outer wall, adjacent to the end of the divertor plate.

The code tracks neutrals from their source, through the edge plasma, until they are ionized. All ionization, scattering, and charge-exchange reactions are included. For this work, the key output of DEGAS2 is the current of neutrals hitting the beryllium first wall. This includes the current to each segment, as well as the energy and incident angle distributions using 20 energy bins between 10 and 1000 eV and 6 angular bins between 0° and 90°.

2.4. VFTRIM-3D deuterium on beryllium sputtering calculations

The VFTRIM-3D (vectorized fractal transport in matter 3D) code simulates surface roughness under the basic TRIM framework [14]. In VFTRIM-3D the surface binding energy applies the heat of sublimation of the material as a key parameter at these low energies. The version of VFTRIM-3D uses an equipartition between the local Oen-Robinson inelastic energy loss model and a non-local Lindhard–Sharff inelastic energy loss model.

Beryllium sputtering has been extensively studied ranging from ion-beam experiments to experiments from magnetized linear plasma devices such as PISCES-B, [15–18]. Fig. 3 shows various experimental and simulation data for deuterium bombardment of beryllium. Experimental data in Fig. 3a is shown in *x*'s and half-filled squares for IIAX data by Ruzic et al. [19], filled squares for Roth et al. [15], which are adjusted to 45° incidence by an empirical formula given by Yamamura et al. [20]. Since in the IIAX experiment beryllium was saturated with deuterium at room temperature, a surface composed of a D/Be ratio of 0.33 was used based on saturation experiments [21]. TRIM-SP simulations use a vectorized version of TRIM-SP known as TRVMCMOM, which uses a binding energy of 1 eV for hydrogen isotopes [22] and beryllium's heat of sublimation of 3.38 eV. This binding energy was also utilized by VFTRIM-3D for consistency.

The data shown in Fig. 3 shows a maximum between 300 and 500 eV, closely resembling BeO data taken by Roth et al. [15]. Beryllium has a high affinity for oxygen at room temperature resulting in binding of

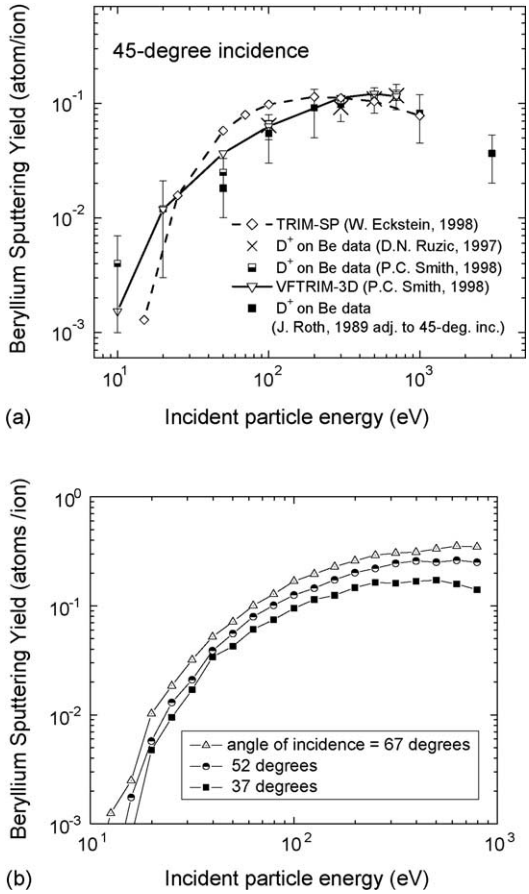

Fig. 3. (a) Beryllium sputtering experimental and computational data for 45° incident D-bombardment; (b) sputtering yields for D^+ on Be from VFTRIM-3D with incident energies between 10 and 1000 eV, and incident angles of 37°, 52°, and 67°.

Be to oxygen lattice sites (heat of formation is equal to −6.3 eV/atom) and thus effectively increasing the surface binding energy of Be atoms, reducing the Be sputtering yield. In addition, the effect of hydrogen isotope implantation in beryllium oxide on beryllium sputtering is important. There is a high likelihood that the affinity of hydrogen isotopes for BeO [23,24] will ultimately lead to a reduction in Be sputtering in general. In addition, the temperature dependence of Be erosion under hydrogen isotope bombardment after forming an oxide is also important. PISCES-B data shows that for temperatures ranging from 25 to 500 °C the sputtering yield of beryllium from bombardment of 100 eV, 10^{18} D^+/cm^2 s^{-1} does not vary much. The measured

data is predicted by TRIM-SP modeling when one assumes a beryllium oxide surface with a surface binding energy of 6.1 eV [18]. Therefore, the difference between sputtering from beryllium and beryllium oxide seems to be small according to both modeling and data [15,18].

Based on the above discussion, VFTRIM-3D simulations were done for the FIRE work here, for pure beryllium, with a fixed surface binding energy of 3.38 eV. Calculations were made for deuterium incident at twenty energies between 10 and 100 eV and six angles between 0° and 90°, in order to exactly match the energy and angle bins used in the DEGAS2 output. Selected yield results are shown in Fig. 3b. These yields are somewhat higher, but in the ballpark of the Fig. 3a data/simulations.

2.5. Combining DEGAS2 and VFTRIM-3D to obtain gross beryllium erosion

We combine the DEGAS2 and VFTRIM-3D results to get the amount of beryllium sputtered from the wall with various energies and angles from each segment of the wall. After the DEGAS2 modeling, we have the ion, neutral, and total deuterium currents to the first wall as a function of energy and angle, $\Gamma_D(E_{in}, \theta_{in})$, for every segment. The VFTRIM-3D results give the beryllium sputtering coefficients, and energy and angular distributions $Y_{Be}(E_{out}, \theta_{out})$ as a function of E_{in} and θ_{in}. For every wall segment, the deuterium flux for every incident energy and angle combination was multiplied by the corresponding sputtering yield distributions. The outgoing beryllium distributions are summed over all incident deuterium energies and angles, finally giving the energy and angular distribution of sputtered beryllium for that wall segment, $\Gamma_{Be}(E_{out}, \theta_{out})$, as needed to study their subsequent transport through the plasma.

2.6. WBC+ beryllium impurity transport

The WBC+ code is a simplified version of the WBC Monte Carlo impurity transport code [25], part of Argonne National Laboratory's REDEP impurity transport package. WBC+ is optimized for fast runs for wall-sputtered material, as opposed to WBC which is used for divertor or limiter sputtered material. WBC+ tracks sputtered impurities from their origin at a first wall surface until they either enter the core plasma, or are redeposited on a wall, divertor, or other surface. (WBC+ is simplified because it lacks the highly detailed sheath treatment, velocity-changing collisions, and certain other aspects of WBC, these being needed for divertors etc. where the plasma flows into the surface along magnetic field lines as opposed to the parallel or near-parallel wall case). In essence, a sputtered beryllium atom leaves the surface and follows a ballistic trajectory until it is ionized. Once ionized, the beryllium follows the magnetic field lines until striking a surface.

The position along the wall for beryllium atoms to be launched is determined randomly, with probability in proportion to the sputtered current for each position along the wall as calculated in Section 2.5. The initial velocity is determined by randomly sampling the energy and angular distributions for that wall segment which, again, are calculated in Section 2.5. The background plasma is specified by the modified UEDGE data generated in Section 2.2.

The final result gives the current of sputtered beryllium to each segment of the first wall itself and to the inner and outer divertor. These currents determine tritium codeposition, and for the divertor the currents serve as input to the erosion modeling of the divertors themselves.

3. Wall sputtering and transport results

Table 1 lists the sputtered and transported beryllium currents for the two cases studied of diffusion-only wall D–T transport, and diffusion plus convection transport. Because the convective flux term was found to domi-

Table 1
Computed beryllium currents for the two cases studied of diffusion-only wall D–T transport, and diffusion plus convection transport (full top-and-bottom wall/divertor system)

Parameter	Diffusion only (#/s)	With convection (#/s)
Sputtered beryllium current, total from wall	8.30×10^{20}	1.62×10^{22}
Be current to inner divertor	3.78×10^{20}	4.30×10^{21}
Be current to outer divertor	1.68×10^{20}	3.10×10^{21}
Be current to inner wall	1.54×10^{19}	3.76×10^{20}
Be current to outer wall	2.70×10^{20}	8.44×10^{21}
Be current to plasma	2.62×10^{17}	2.18×10^{18}

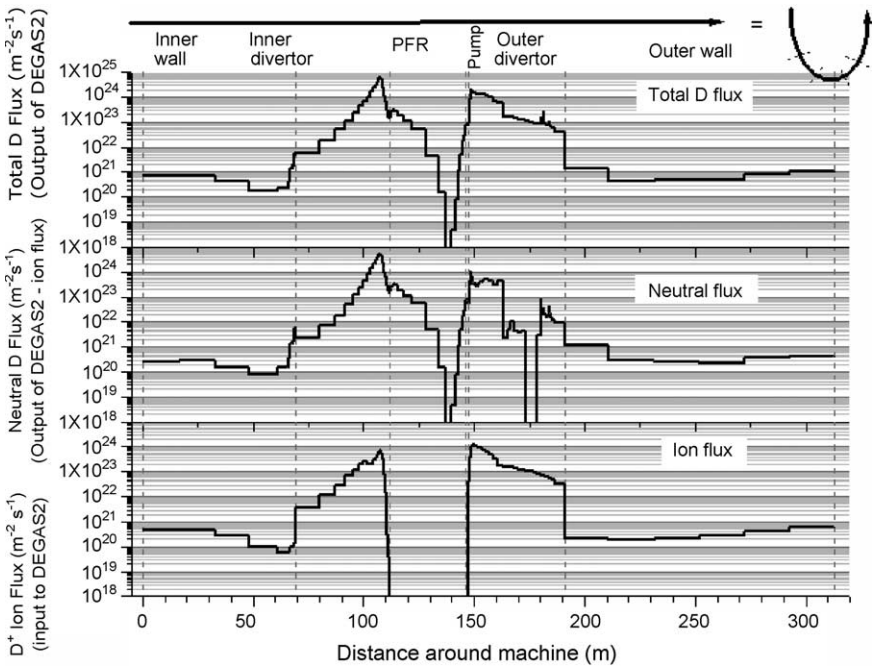

Fig. 4. The fluxes of deuterium to the walls/divertors all the way around the FIRE tokamak. The bottom panel shows the flux of D^+ which served as the input to the DEGAS2 calculations. The top panel gives the output of DEGAS2, which is the combined ion and neutral flux. Finally, the middle panel is the contribution of just neutrals, calculated as the output from DEGAS2 minus the input. Fluxes shown are for the case without convective transport.

nate the calculated ion flux to the first wall, and hence the resulting beryllium fluxes, the two cases will be discussed separately.

3.1. Diffusive transport only

The results of the neutral modeling for this case are shown in Fig. 4. In this case, the peak deuterium flux to the first wall is $1.35 \times 10^{21}\ m^{-2}\ s^{-1}$, occurring at the location of the gas puffing. The total deuterium current to the first wall is $3.48 \times 10^{22}\ s^{-1}$, for an average flux of $7.11 \times 10^{20}\ m^{-2}s^{-1}$. The average energy of incident deuterium ions and neutrals is 48 eV.

When the sputtering coefficients as described in Section 2.5 are taken into account a total beryllium sputtering source is calculated to be $8.30 \times 10^{20}\ s^{-1}$. This corresponds to an overall sputtering yield of 2.4%. This is a reasonable value based on the VFTRIM results. Of this source, WBC+ finds that 66% of the sputtered beryllium reaches the inner and outer divertor system.

3.2. With convective transport added

With the convective transport term added to the model used to calculate the ion flux to the first wall, the peak deuterium flux increases by an order of magnitude to $1.75 \times 10^{22}\ m^{-2}\ s^{-1}$. Fig. 5 shows that the deuterium flux is also more evenly distributed along the wall, although the location of the gas puffing still receives the highest flux. The total current to the first wall is about 16× higher than the previous case, at $5.62 \times 10^{23}\ s^{-1}$, with the average flux being $1.15 \times 10^{22}\ m^{-2}\ s^{-1}$. The average deuterium energy is similar to the previous case, at 52 eV.

The sputtering calculations give a total beryllium sputtering source of $1.62 \times 10^{22}\ s^{-1}$, some 20 times larger than without convection. The extra increase is due to the slightly higher average energy of incidence, since the average sputtering yield increases to 2.9%.

In this case, 46% of the beryllium atoms launched in WBC+ make it to the divertor. The difference in transport properties is due to different sputtered energy

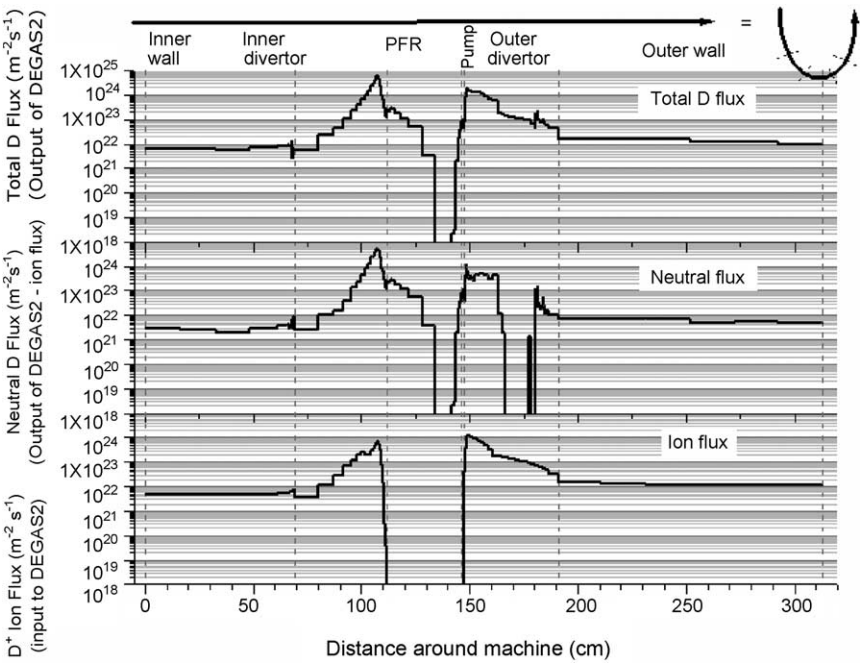

Fig. 5. The fluxes of deuterium to the walls/divertors all the way around the FIRE tokamak, with the same orientation as Fig. 4 with convective transport included.

and angular distributions, e.g. beryllium sputtered at a higher energy is more likely to not be locally redeposited and reach the divertor.

The net erosion rate (sputtering minus redeposition) for the outer and inner wall is shown in Figs. 6 and 7, respectively. Beryllium and deuterium ion fluxes to the divertor are shown in Figs. 8 and 9. Also shown is the plasma convective heat flux-this is important to assess surface temperature for tritium codeposition analysis.

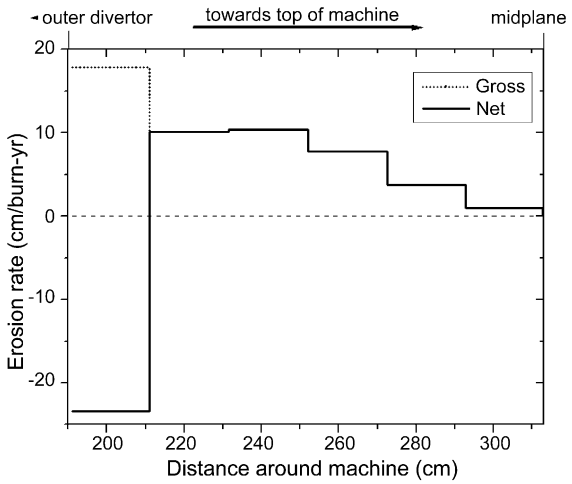

Fig. 6. Net erosion rate, outer wall, for convective transport case.

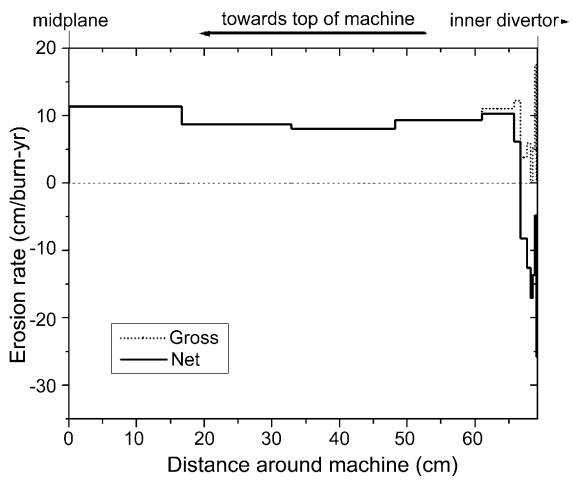

Fig. 7. Net erosion rate, inner wall, for convective case.

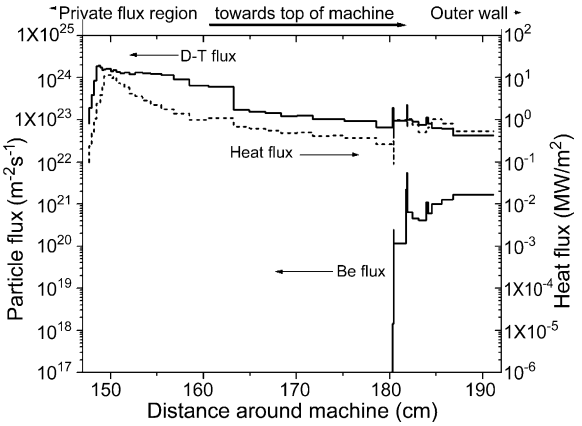

Fig. 8. Flux of beryllium to outer divertor, for convective case. Also shown is the D–T ion flux and the plasma convective heat flux.

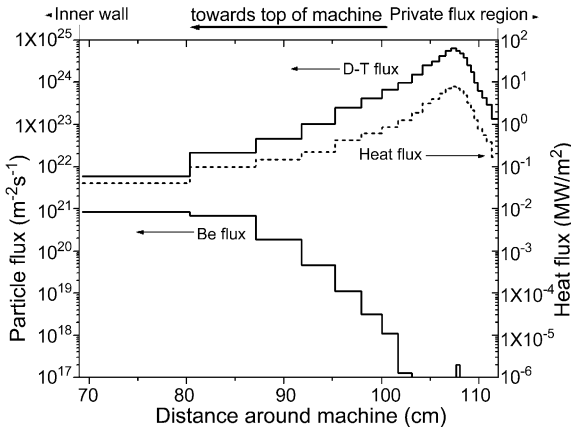

Fig. 9. Flux of beryllium to inner divertor, for convective case. Also shown is the D–T ion flux and the plasma convective heat flux.

Wall erosion profiles and divertor fluxes for the no-convection case have fairly similar shapes with about 10 times lower values.

4. Core plasma contamination

The beryllium core plasma contamination depends on the input source to the core, I_{Be} and the core plasma particle transport. The latter can be globally categorized by the core plasma particle confinement time, τ. The core beryllium ion content, N_{Be}, reaches an equilibrium when $N_{Be}/\tau = I_{Be}$. (This uses the fact that Be outflux from the core would not significantly recycle due to sticking on divertor surfaces.) Using a ballpark estimate of $\tau = 1$ s and total number of fuel particles in the plasma of 1×10^{22} [26,27] and the WBC+ code computed current to the core, the equilibrium core plasma concentration ratio is $n_{Be}/n_{DT} = 2 \times 10^{-4}$ for the convection case, and about 10 times less for the diffusion-only case. These are very low. We have not included here beryllium transport to the core from sputtering of the *divertor* surface which is expected to be low.

5. Divertor response

As seen in Figs. 8 and 9, there is a substantial direct flux of wall-sputtered beryllium to both inner and outer divertors. This occurs away from the respective strike points. At and near the strike points there will be an indirect flux of beryllium arising from wall-to-plasma-to-divertor transport. The magnitude of this indirect flux is dependent on the core beryllium concentration, such concentration estimated in the previous section. These two sources of beryllium flux to the divertor raise the question of what happens to the initially-tungsten divertor surface. A companion study has analyzed the mixed material response of the FIRE divertor, at the outer divertor strike point [28] Using estimates of beryllium currents to the divertor from this work as input, the ITMC binary collision mixed-material code was used to compute Be/W surface evolution and sputter response. The results show that under most conditions beryllium will simply build up over the tungsten. Thus, at least between transients such as disruptions, the tungsten surface will essentially turn into a beryllium surface. (ELM response of the Be surface can also play a role—this has not been analyzed).

The full WBC Monte Carlo impurity transport code was then used for this study to further examine some aspects of divertor beryllium erosion/redeposition. A detailed analysis is beyond the scope of this work, i.e. to calculate full spatially-resolved sputtered material transport, but we have identified the basic trends at selected divertor points. Table 2 summarizes WBC results for the strike point case and one other point. A key result is that at the outer divertor strike point, sputtered Be is highly redeposited, essentially 100%, as with tungsten. This is due to the very high electron density, with the high magnetic field (10 T) also a factor.

Table 2
Selected erosion/redeposition parameters from WBC analysis of FIRE outer divertor w/beryllium surface, at strike point and away from strike point

Parameter[a]	At strike point[c]; $T_e = 15$ eV; $n_e = 2.17 \times 10^{21}$ m^{-3}	7 cm from strike point; $T_e = 4$ eV; $n_e = 3 \times 10^{21}$ m^{-3}
Neutral ionization distance[b] (mm)	0.15	0.61
Energy (eV)	74	39
Transit time (μs)	0.11	0.83
Elevation angle (°)	34	51
Charge state	1.4	1.2
Redeposition fraction (for 1 cm near-surface cutoff)	1.00	0.90

[a] Except where noted denotes average value for redeposited beryllium ions.
[b] Normal to surface.
[c] Using a somewhat different plasma solution than for neutrals calculation.

Away from the strike point, there is high redeposition also, for about $T_e > 4$ eV, due to the high electron density. Redeposition fractions fall off sharply, however, for lower electron temperature divertor regions, due to the steep falloff in electron impact ionization rate coefficient, but in these regions the sputter yields diminish rapidly as well. At the inner divertor, for the plasma case studied, the impinging ion energy for D^+, T^+, is below the sputtering threshold though there could be sputtering, not-assessed, by charge exchange neutrals, and trace oxygen, neon, etc. ions.

Although not assessed in detail here, based on the present results and on previous divertor/SOL-plasma studies, transport to the FIRE core plasma from divertor sputtering should be low. Some sputtered divertor material could go to other surfaces, such as the baffle, though this does not appear to be of major consequence. For the present purposes of estimating codeposition, for the above stated reasons, we can assume buildup of beryllium on the divertor.

6. Tritium codeposition

Tritium codeposition can occur on FIRE surfaces subject to beryllium buildup with concurrent tritium ion/atom impingement. These surfaces are seen here to be the outer wall and the inner and outer divertors. Extensive studies of hydrogen isotope retention/trapping in beryllium have been conducted and the reader is referred to the literature for details [21,23,24,29–33]. In particular, tritium codeposition in beryllium has been reviewed by Causey and Walsh [31,32]. While pure Be has low trapping rates, the controlling factor is the presence of plasma background oxygen.

Oxygen traps hydrogen isotopes in BeO form. The retention of hydrogen isotopes (D) in BeO leads to the formation of the hydroxide, BeOD, according to the reaction:

$$2\mathrm{BeO} + 2\mathrm{D} \rightarrow \mathrm{Be(OD)_2} + \mathrm{Be} + \frac{0.704\ \mathrm{eV}}{\mathrm{D}}$$

also leading to the release of free Be, which in turn reacts with residual oxygen growing an oxide layer.

Oxygen is present in all tokamaks and nearly all lab experiments. Oxygen appears to be introduced primarily from vacuum vessel and related structure outgassing. While high duty factor devices, operated with extended hot surfaces, could possibly reduce oxygen levels to below influence levels for beryllium codeposition this seems unlikely in FIRE.

For any oxygen content, the codeposition trapping rates vary strongly with surface temperature. Reported rates are as high as Q/Be ∼0.35 at rt., which is similar to carbon. A temperature of 527 °C is reported for little or no trapping and/or driving out previously trapped hydrogen [15]. To compute codeposition here we use two Q/Be rates for scoping purposes, first from Mayer et al. data for “abundant” oxygen [29,30], and Causey and Walsh for low/zero oxygen [31,32].

As seen in Figs. 8 and 9 the flux of plasma fuel ions is everywhere much greater than the Be flux, hence, D–T will be trapped up to the Q/Be ratio for

Table 3
Tritium codeposition estimates

D–T ion flux to wall transport assumption	Q/Be trapping data assumption	Codeposition rate	No. of 20 s shots needed to reach 1 gT
With convection	Mayer et al.[a] ("abundant" oxygen)	1.93×10^{21} T s^{-1} = 9.68 mg T s^{-1}	5
With convection	Causey and Walsh[b] (low/no oxygen)	3.22×10^{20} T s^{-1} = 1.61 mg T s^{-1}	31
Diffusion only	Mayer et al.[a] ("abundant" oxygen)	1.08×10^{20} T s^{-1} = 0.542 mg T s^{-1}	92
Diffusion only	Causey and Walsh[b] (low/no oxygen)	1.80×10^{19} T s^{-1} = 0.0903 mg T s^{-1}	554

[a] Q/Be ∼ 0.3 @ 250 °C [29,30].
[b] Q/Be ∼ 0.05 @ 250 °C [31,32].

the surface temperature in question. Tritium will constitute half the trapping. It is seen from Figs. 6–9 that codeposition can occur on the outer wall, inner and outer divertors, where there is a growth of beryllium, but not on the inner wall where there is net erosion only.

There is limited surface temperature information available for the various surfaces in FIRE. A peak front surface temperature of 220 °C has been estimated for the inner divertor for baseline 10 T shots [26,27]. Recent analysis [34,35] using various plasma heating profiles shows inner divertor surface temperatures varying along the surface from about 50 °C to about that same peak value of 220 °C. Outer divertor temperatures have been estimated, varying from about 80 °C for divertor regions with heat loads of ∼1 MW m^{-2}, to ∼450 °C for ∼7 MW m^{-2} to well over 1000 °C for higher heat loads [26,27,34,35]. The coldest spots will be about at room temperature. First wall temperature estimates vary widely depending on assumed power loading and active versus passive cooling. Due to the numerous variations—as is reasonable for an evolving conceptual design like FIRE—we estimate codeposition ratios here using a rough estimate approach where there is either (A) no deposition due to very high surface temperature, or (B) there is deposition at a fixed, lower temperature.

For both the inner and outer divertors the direct wall-to-divertor beryllium current is deposited in regions of low heat flux, see Figs. 8 and 9. As discussed, there will be an additional current from wall-to-plasma-to-divertor transport. The peak outer divertor temperature, occurring at the strike point, is clearly high enough for no codeposition to occur or if it does occur early in the pulse the hydrogen isotopes will be driven out by the end of the pulse. Therefore, we ignore codeposition on the hot, near strike point portion of both divertors, and compute codeposition on the "cold" parts. Likewise, we compute codeposition for the outer wall using the assumption of a "cold" surface.

For scoping purposes we use a temperature of 250 °C for these "cold" regions. Table 3 shows T/Be codeposition rates for this temperature, and using the two Q/Be ratios corresponding to different oxygen conditions.

Codeposition rates very substantially. For the worst case of convection/ample-oxygen, codeposition rates are very high and would require major amelioration and rethinking of the design. (For example by somehow designing for transient high-heating of the "cold" surfaces). Also, since the trapping rates approach the tritium fueling rate of 1 to 2×10^{21} s^{-1} [26,27], this would raise questions of the effect of removal of this much T (and D) on the edge plasma itself. Clearly, reliable predictive rates for this case would have to be more rigorously computed. For the best case of no-convection/low-oxygen, codeposition rates appear to present no major difficulties to FIRE operation.

A further note is that because the beryllium current to the core is so low it would not serve the purpose of increasing SOL/edge radiation. Some FIRE scenarios call for beryllium to be *added* to the plasma, to radiate power thereby minimizing peak convective power. Such addition would raise concern about further increasing the codeposition rates.

7. Discussion

Since the impurity levels in the SOL and edge plasma are low for the cases studied this is not a problem-in terms of self-consistency for the basic plasma solution. There is a self-consistency concern regarding the convective flow calculations. Specifically,

because the convective transport is large, it may not be accurate to assume that the original UEDGE solution will remain unchanged. This comment also applies to the highest cases of D–T particle removal via codeposition. It should be noted that there are other major issues connected with the convection issue particularly heat loading of the wall. Work is needed on (1) physics of convective transport, (2) effect on the design. There is an obvious need for future, self-consistent calculations to address these issues. Future work should also analyze the effect of detached plasmas versus the studied attached-plasma regime.

8. Conclusions

This work represents a state-of-the-art attempt at computation of a highly complex subject, that of wall material erosion/transport/codeposition, combining numerous plasma and plasma-material interaction codes. Although there are necessarily some inconsistencies, the results should enable reasonable evaluation of beryllium wall performance issues for next generation fusion tokamaks, i.e., ignition devices and/or similar near-term devices (ITER).

The FIRE beryllium coated first wall is predicted to work well from the plasma contamination standpoint, with essentially all but a trace amount of wall-sputtered beryllium depositing on the divertors or back on the wall. Wall erosion rates are high, for the plasma regime studied, but tolerable due to the low duty-factor. Erosion is high due to high fluxes of D–T ions/atoms, high sputter yields for beryllium, and relatively low local redeposition.

A large fraction of wall-sputtered material goes to the inner and outer divertor. The divertor surfaces, nominally tungsten, would become in situ coated with beryllium, as least between plasma high power transients.

A key concern is tritium codeposition in redeposited growth areas of beryllium. This is highly dependent on whether or not convective transport of D–T ions to the wall occurs. It is also dependent on background oxygen level and surface temperatures. In the best case tritium codeposition in FIRE appears to be acceptable and in the worst case is unacceptable.

An outstanding question for FIRE or like device is whether beryllium is actually needed on the wall. Based on a rough extrapolation of the beryllium results here for iron, a stainless steel (Fe) wall would not impair plasma performance through sputtering, and would avoid tritium codeposition concerns.

Acknowledgements

We would like to thank Tom Rognlien (LLNL) and Marv Rensink (LLNL) for providing the UEDGE plasma solution and for numerous discussions, and Rion Causey (SNL) for discussions about beryllium codeposition.

References

[1] J.N. Brooks, Modeling of sputtering erosion/redeposition-status and implications for fusion design, Fusion Eng. Des. 60 (2002) 515.
[2] D.M. Meade, FIRE, a next step option for magnetic fusion, Fusion Eng. Des. 63–64 (2002) 531.
[3] J.N. Brooks, D.N. Ruzic, D.B. Hayden, Sputtering erosion of beryllium coated plasma facing components-general considerations and analysis for ITER detached plasma regime, Fusion Eng. Des. 37 (1997) 455.
[4] M.A. Ulrickson, J.N. Brooks, D.E. Driemeyer, et al., Physics basis for the fusion ignition research experiment plasma facing components, Fusion Eng. Des. 58–59 (2001) 907.
[5] T.D. Rognlien, J.L. Milovich, M.E. Rensink, et al., J. Nucl. Mater. 196–198 (1992) 347.
[6] M.E. Rensink, T.D. Rognlien, UEDGE results, LLNL, personal communication, 2001, 2002. 2003.
[7] D.N. Ruzic, D. Heifetz, S. Cohen, The density dependence of neutral hydrogen density and neutral hydrogen emission from PLT, J. Nucl. Mater. 145–147 (1987) 527.
[8] H.Y.W. Tsui, A.J. Wooton, et al., A database for edge turbulence and transport studies, J. Nucl. Mater. 196–198 (1992) 794.
[9] R.D. Monk, L.D. Horton, A. Loarte, G.F. Matthews, P.C. Stangeby, Determination of JET scrape-off layer transport coefficients using an interpretive onion-skin plasma model, J. Nucl. Mater. 220–222 (1995) 612.
[10] G.Y. Antar, et al., Experimental evidence of intermittent convection in the edge of magnetic confinement devices, Phys. Rev. Lett. 87 (6) (2001).
[11] M. Kotschenreuther, T. Rognlien, P. Valanju, Implications of convective scrape-off layer transport for fusion reactors with solid and liquid walls, Fusion Eng. Des. 72 (2004) 169.
[12] D. Stotler, C. Karney, Contrib. Plasma Phys. 34 (1994) 392.
[13] D. Heifetz, D. Post, M. Petravic, et al., J. Comput. Phys. 46 (1982) 309.
[14] D.N. Ruzic, The effects of surface roughness characterized by fractal geometry, Nucl. Instrum. Methods Phys. Res. B47 (1990) 118.

[15] J. Roth, W. Eckstein, M.I. Guseva, Erosion of Be as plasma-facing material, Fusion Eng. Des. 37 (1997) 465.
[16] R.W. Conn, R.P. Doerner, J. Won, Beryllium as the plasma-facing material in fusion energy systems—experiments, evaluation, and comparison with alternative materials, Fusion Eng. Des. 37 (1997) 481.
[17] P.C. Smith, D.N. Ruzic, Low energy (10 to 700 eV) angularly resolved sputtering yields for D+ on beryllium, Nucl. Fusion 38 (5) (1998) 673.
[18] R.P. Doerner, A. Grossman, S. Luckhardt, R. Seraydarian, F.C. Sze, D.G. Whyte, R.W. Conn, Response of beryllium to deuterium plasma bombardment, J. Nucl. Mater. 257 (1998) 51.
[19] D.N. Ruzic, P.C. Smith, R.B. Turkot Jr., Measurements and modeling of the angular-resolved sputtering yield of D-soaked Be by 100, 300, 500 and 700 eV D+, J. Nucl. Mater. 241–243 (1997) 1170.
[20] Y. Yamamura, Y. Itikawa, N. Itoh, Angular dependence of sputtering yields of monoatomic solids, IPPJ-AM-26 (Institute of Plasma Physics, Nagoya, Japan) (1983).
[21] J.N. Brooks, R. Causey, G. Federici, D.N. Ruzic, Assessment of erosion and surface tritium inventory issues for the ITER divertor, J. Nucl. Mater. 241 (1997) 294.
[22] W. Eckstein, Sputtering, reflection and range values for plasma edge codes, IPP Report 9/117 (1998).
[23] R.A. Causey, J.N. Brooks, G. Federici, Tritium inventory and recovery in next-step fusion devices, J. Nucl. Mater. 61–62 (2002) 525.
[24] V.M. Sharapov, V.Kh. Alimov, L.E. Gavrilov, Deuterium accumulation in beryllium oxide layer exposed to deuterium atoms, J. Nucl. Mater. 258–263 (1998) 803.
[25] J.N. Brooks, Near-surface sputtered particle transport for an oblique incidence magnetic field plasma, Phys. Fluids B-Plasma Phys. 2 (1990) 1858.
[26] FIRE Engineering Status Report for Fiscal Year 2000. Report No. 81-001030 (Oct. 2000), Princeton Plasma Physics Laboratory.
[27] FIRE Engineering Status Report for Fiscal Year 2001, Report No. 81-0010202 (Jan. 2002), Princeton Plasma Physics Laboratory.
[28] A. Yacout, A. Hassanein, Modeling and analysis of mixed-material surface evolution and sputtering, PSI-16, J. Nucl. Mater. (in press).
[29] M. Mayer, et al., Codeposition of hydrogen with Be, C, and W, J. Nucl. Mater. 230 (1996) 67.
[30] M. Mayer, Codeposition of deuterium with BeO at elevated temperatures, J. Nucl. Mater. 240 (1997) 164.
[31] R.A. Causey, D.S. Walsh, Codeposition of deuterium with beryllium, J. Nucl. Mater. 254 (1998) 84.
[32] R.A. Causey, Hydrogen isotope retention and recycling in fusion reactor plasma-facing components, J. Nucl. Mater. 300 (2002) 91.
[33] R.A. Anderl, R.A. Causey, J.W. Davis, R.P. Doerner, G. Federici, A.A. Haasz, et al., Hydrogen isotope retention in beryllium for tokamak plasma-facing applications, J. Nucl. Mater. 273 (1999) 1.
[34] C.B. Baxi, M.A. Ulrickson, D.E. Driemeyer, P. Heitzenroed, Thermal hydraulic analysis of FIRE divertor, Fusion Technol. 39 (2) (2001) 412.
[35] M.A. Ulrickson, SNL, personal communication (2003).